Lunar Reconnaissance Orbiter K-Band (26 GHz) Signal Analysis: Initial Study Results

David D. Morabito* and David Heckman*

ABSTRACT. — Lower frequency telemetry bands are becoming more limited in bandwidth due to increased competition between flight projects and other entities. Higher frequency bands offer significantly more bandwidth and hence the prospect of much higher data rates. Future or prospective flight projects considering higher frequency bands such as Ka-band (32 GHz) for deep-space and K-band (26 GHz) for near-Earth telemetry links are interested in past flight experience with available received data at these frequencies. Given that there is increased degradation due to the atmosphere at these higher frequencies, there is an effort to retrieve flight data of received signal strength to analyze performance under a variety of factors. Such factors include elevation angle, season, and atmospheric conditions. This article reports on the analysis findings of over 10 million observations of received signal strength of the Lunar Reconnaissance Orbiter (LRO) spacecraft collected between 2014 and 2017. We analyzed these data to characterize link performance over a wide range of weather conditions, season, and as a function of elevation angle. Based on this analysis, we have confirmed the safety of using a 3-dB margin for preflight planning purposes. These results suggest that a 3-dB margin with respect to adverse conditions will ensure a ~98 to 99 percent data return under 95 percent weather conditions at 26 GHz (K-band), thus confirming expectations from link budget predictions. The results suggest that this margin should be applicable for all elevation angles above 10 deg. Thus, missions that have sufficient power for their desired data rates may opt to use 10 deg as their minimum elevation angle. Limitations of this study include climate variability and the fact that the observations require removal of hotbody noise in order to perform an adequate cumulative distribution function (CDF) analysis, which is planned for a future comprehensive study. Flight projects may use other link margins depending upon available information, uncertainties of non-atmospheric link parameters, and mission phase.

I. Introduction

Ka-band (32 GHz) and K-band (26 GHz) offer several advantages for received downlink telemetry and navigation over lower frequency bands such as wider spectrum allocation, higher antenna gain, and greater immunity to plasma effects. These make for possible

* Communications Architectures and Research Section.

The research described in this publication was carried out by the Jet Propulsion Laboratory, California Institute of Technology, under a contract with the National Aeronautics and Space Administration.

increased performance and greater accuracy for navigation data types. Early deep-space Ka-band experiments and demonstrations included Mars Observer, Mars Global Surveyor, Deep Space 1, and Mars Reconnaissance Orbiter. Mars Observer was the first demonstration of a deep-space communications link and had an active Ka-band campaign from 1993 to 1994. More recent deep-space Ka-band flights include Cassini [1] and Kepler, with the analysis of its signal strength data reported in a companion article in this volume [2].

Lunar Reconnaissance Orbiter (LRO) has been orbiting the Moon in a polar orbit since 2009, and has been performing detailed mapping of the lunar surface as well as conducting other measurements. The spacecraft was launched on June 18, 2009, and entered lunar orbit on June 23, 2009. The status of the processing of received signal data from the White Sands 18-m-diameter station (designated WS1) is reported on here in this article focusing on the 26-GHz near-Earth K-band allocation used for high-rate science data downlink. This is a preliminary status report pending several caveats discussed later in this article.

II. Observations

LRO orbits the Moon in a near-circular orbit with an approximate 50-km altitude with a ~2-hr period. About six tracking passes per day are conducted using the 18-m White Sands antenna, each of duration ~1 hr. LRO has an S-band link (2.2 GHz) used primarily for low-rate engineering data and a K-band link (25.65 GHz) used for high-rate science data. The K-band system has a 40-W transmitter and a 75-cm-diameter high-gain dish antenna, which provides a downlink consisting of high-rate telemetry data at 100 Mbps in two orthogonal channels of 50 Mbps each. The nominal values for parameters used in the link budget analysis for the LRO spacecraft and for the White Sands ground station were from [3].

The models used for atmospheric statistics in the link budgets are based on International Telecommunication Union (ITU) models ([4] references therein) and the weather statistics input to the models are based on results reported in [4]. The atmospheric model used in the favorable link budget calculations assumed 50 percent availability, while the atmospheric model used in the adverse link budget calculations assumed 95 percent availability.

The lunar hotbody contribution to the system noise temperature used in link calculations was derived from lunar brightness temperature maps at several lunar phase values at 26 GHz.[1] The disk-center values of lunar brightness temperature as a function of lunar phase angle are plotted in Figure 1, where 180 deg represents full Moon and 0 deg represents new Moon. The peak of the curve lies about 30 deg later than full Moon due to latent heating of the lunar surface at this frequency. As inferred from Figure 1, the maximum value of brightness temperature, 275 K, represents a worst case or adverse value. The conversion of brightness temperature to its contribution to system noise temperature uses models provided by [5]. For the adverse link budget calculations, we assume a maximum brightness temperature of 275 K applicable when LRO is near the lunar disk center (such as during a diametric crossing). For the favorable link budget calculations, we assumed a

[1] Provided by Stephen Keihm (now retired), personal communication, Jet Propulsion Laboratory, Pasadena, California, April 2014.

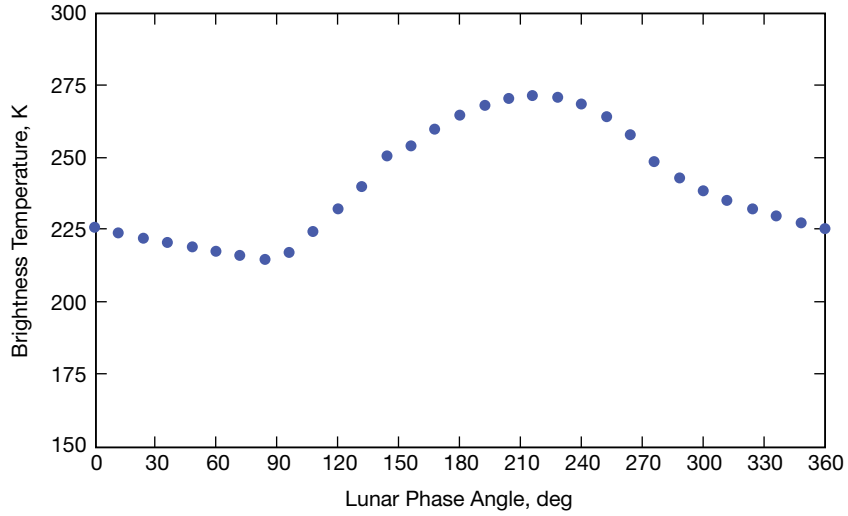

Figure 1. Lunar brightness temperature at 26 GHz as a function of lunar phase angle where 180 deg is full Moon and 0 deg is new Moon.

brightness noise temperature of about 42 percent of this value applicable when LRO is near the lunar limb (such as during a "grazing" orbit). This assumption makes use of a comparison of disk-centered and limb-centered measurements performed at similar frequency and antenna size [6].

The range distance between White Sands and the LRO spacecraft over the ~2-yr period of the observations varied with a monthly periodicity, as shown in Figure 2. The minimum range distance used in the favorable link budget calculations was 354,152 km and the maximum range distance used in the adverse link budget calculations was 411,154 km. This contributes to a 1.3-dB spread in received signal strength between nearest and farthest range distances, which is reflected in the link budget curves to be presented later with the raw observations of received E_b/N_0 at White Sands.

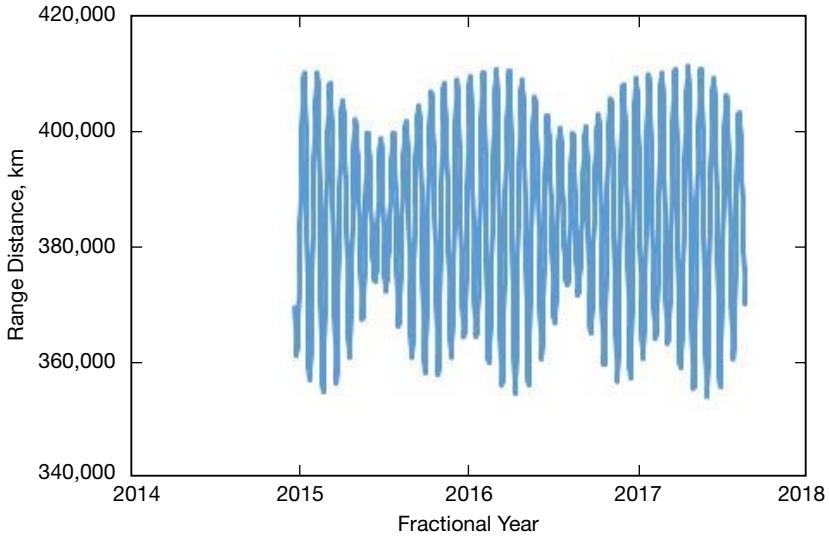

Figure 2. LRO to White Sands range distance.

We started receiving regular data deliveries from the project on year 2016 on day of year 161 (2016-161) after the completion of each tracking pass. A request was later made to acquire previous data. No data were available prior to June 2014, and there were not any E_b/N_0 measurements available prior to December 2014. The first set of data files for 2014 (see the first row of Table 1 and Figure 7 later in this article) contained a limited number of E_b/N_0 observations acquired during testing performed at the White Sands WS1 station. The gap between December 2014 and mid-2015 was the length of time it took to finish addressing issues found during the testing. During that intervening period, some data were collected but did not include E_b/N_0 measurements and other pertinent data. Thus, the primary data set includes data acquired from mid-2015 to about mid-2017.

For this study, we chose the energy-to-noise ratio per unit bit E_b/N_0 as the signal parameter in which to characterize the performance of the link. Figure 3 displays an example of the behavior of E_b/N_0 versus time during a typical tracking pass.

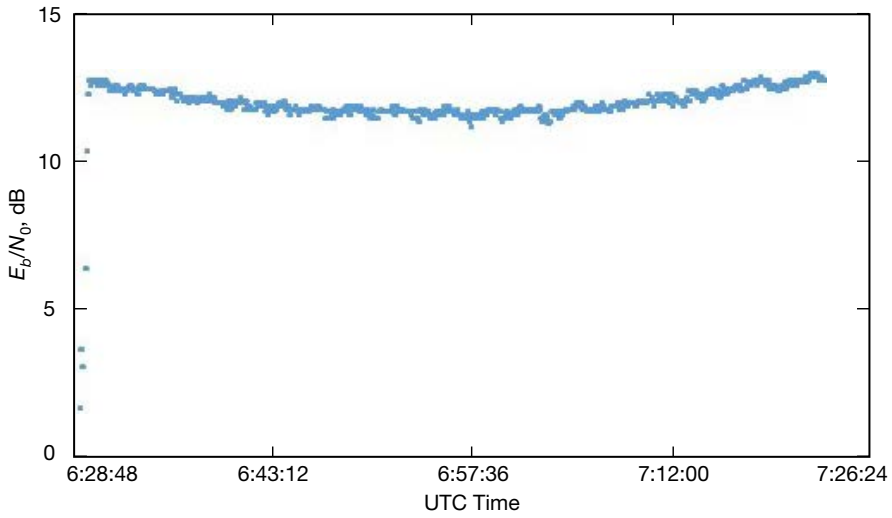

Figure 3. Received E_b/N_o versus time signature for a typical tracking pass, which occurred on January 15, 2017 (orbit 34089).

Figure 4 depicts the average E_b/N_0 over each tracking pass orbit starting from 2016-161. Each blue data point in Figure 4 represents the average E_b/N_0 over each tracking pass of ~1 hr duration. The red curve in Figure 4 represents the minimum angle of LRO's orbital trace relative to lunar disk center during each tracking pass. Note that when the angle ~>90 deg (see right-hand vertical axis), the orbit is nearly face-on (see Figure 5). In this case, there is minimum lunar hotbody noise contribution to the E_b/N_0 measurements and thus the peaks of the average E_b/N_0 occur here. When this angle ~0 deg, the orbit is nearly disk-center crossing (see Figure 6), and thus we get maximum contribution to the lunar hotbody noise contribution to the E_b/N_0 measurements. Thus the "minimums" of the average E_b/N_0 measurements usually occur here. Some of the average E_b/N_0 measurements that lie below ~11 dB have been correlated with periods of antenna mispointing, or periods of significant atmospheric degradation. There is a two-week periodicity between face-on and disk-center crossing orbits (see Figure 4) resulting in about ~2 dB peak-to-peak variation in average E_b/N_0 due primarily to the different contributions of hotbody noise and range distance.

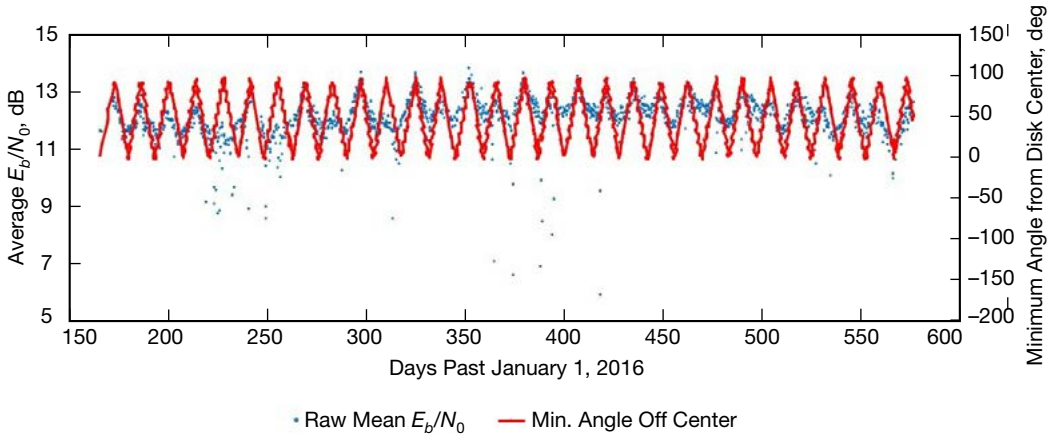

Figure 4. Average of E_b/N_0 measurements over each tracking pass (blue dots) along with minimum angular distance from orbit trace to center of lunar disk (red curve).

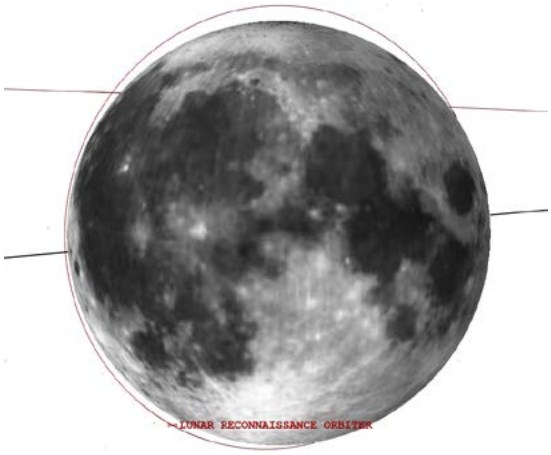

Figure 5. Example of where LRO is in a near face-on orbit where hotbody noise contribution is near minimum. Here, minimum angle of orbit to center of lunar disk would be ~90 deg.

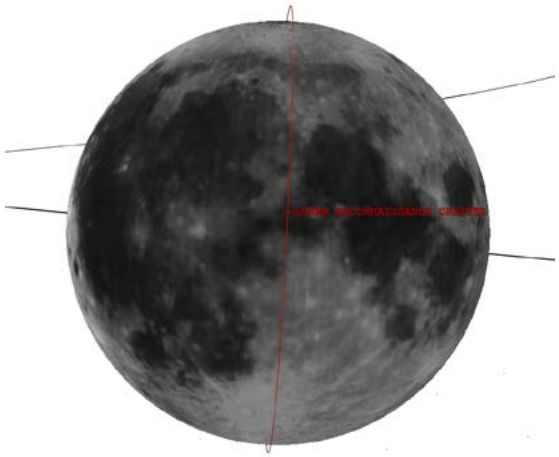

Figure 6. Example of where LRO is in a near disk-center crossing orbit where hotbody noise contribution is near maximum. Here, minimum angle to center of lunar disk is <2 deg.

III. Analysis of Individual E_b/N_0 Observations

Given that important short time-scale features are "washed-out" in the averages plotted in Figure 4, it is important to analyze the individual sampled observations of received signal strength, so that their statistical significance can be assessed. The individual E_b/N_0 measurements were sampled at 1-s time resolution. This results in ~3600 data points for each ~1-hr tracking pass. Given there can be approximately six tracking passes per day over the course of the several-year period, there were found to be over 10 million such observations (after removing obviously erroneous data points). Since there were so many of these measurements, we examined them in batches (Figures 7 to 27 on pages 9–15 display these results for each batch from December 2014 to August 2017). These plots display the individual E_b/N_0 measurements (blue dots) as a function of elevation angle for each batch of data processed. It is emphasized that no attempt was made to adjust the individual E_b/N_0 measurements for any differences in link parameters in order to preserve the originality of the data. Instead, we compare with adverse and favorable link assumptions by overlaying these plots with the appropriate curves. Therefore we have plotted in these figures the adverse (red curve) and favorable (black curve) link budget curves. The dashed yellow curves on each plot represent the 3-dB margin curve lying below the adverse curves.

Table 1 (page 8) displays the start and stop dates (first and second columns) for each batch of data displayed in the plots along with the total number of observations (third column) and the number of observations lying above the dashed yellow 3-dB curves (fourth column). The fifth column displays the percentage of data lying above the 3-dB curves for each batch of data. We see that for all cases more than 98 percent of the data lie above the 3-dB curves. The bottom row summarizes the overall statistical comparison, where 99.2 percent of the data consisting of over 10 million 1-s observations lie above the 3 dB curves.

The black solid curves in Figures 7 to 27 represent the E_b/N_0 versus elevation angle dependence based on "favorable" link assumptions, which include minimum range distance, minimal hotbody noise, and nominal atmospheric conditions (50 percent availability). Note that these curves do a generally good job of bounding the upper envelope of the E_b/N_0 data points, although based on statistical expectations we expected a certain percentage of points to lie above the favorable curve. More discussion on this will be provided later. We suspect that there may be a small elevation dependence of the ground antenna gain in vacuum conditions, but such a model was not available. Such a model may cause the link curves to bend down slightly at higher elevation angles.

The red solid curves in Figures 7 to 27 represent the E_b/N_0 versus elevation angle dependence based on adverse link assumptions, which include maximum range distance, maximum hotbody noise (disk-center crossing orbit), and adverse atmospheric conditions (95 percent availability). Note that these curves do a good job of bounding almost all the E_b/N_0 data points falling near the bottom of the main ~2 dB extent of the envelope of the raw observations up to the favorable link curve, corresponding to the limits of hotbody noise, atmospheric loss, and range distance.

The dashed yellow curve represents the link corresponding to 3 dB below the adverse curve. Table 1 itemizes the number of data points and percentage of them that lie above this curve

for each batch of data. It should be noted that the "Adverse – 3 dB Curve" corresponds to a percent weather somewhat greater than 99 percent. This means that if all other link budget parameters were known with great certainty, then only atmospheric effects would dominate and that less than 1 percent of the points would fall below this curve, which is close to what is observed.

The blue E_b/N_0 data points in Figures 7 to 27 that lie below the dashed yellow curves fall into two main categories. First, the data points that appear to be connected showing trends are more likely due to atmospheric-induced fade features, or (less likely) antenna (either spacecraft or ground) mispointing signatures not yet removed from the data sets. Non-atmospheric-induced signatures remaining in the data sets would be expected to be identified and removed, but their removal is not expected to significantly change the numerical conclusions. Second, the data points that appear scattered and not connected are likely due to periods of high winds, during maneuvers, during signal acquisition (see very start of Figure 3), or during loss of signal at end of track. These are more difficult to delete as they would require "removal by hand." In any event, about 99 percent of the data points lies above this curve and removal of non-weather-related events is not expected to significantly change the statistics nor the general conclusions.

The percentage of data points lying above the "Adverse – 3 dB" curve is similar from batch to batch, generally running at the 98 to 99 percent levels, as is apparent from inspection of Table 1. We analyzed a total of 10,403,361 data points, of which 10,324,319 lie above the "Adverse – 3 dB" curve (99.2 percent).

The E_b/N_0 measurements plotted in Figures 7 to 27 are the raw measurements reported by the receiver. No adjustments were made to the E_b/N_0 data in range distance, weather, or hotbody noise. We have tested a model in which a coarse hotbody noise contribution is removed from the E_b/N_0 measurements. This adjustment tends to reduce the spread (or envelope) of the measurements as expected, but we prefer to report on the raw measurements here in this article. Lunar hotbody noise model removal as well as adjusting all measurements to a common range distance are focuses of future study.

The strange behavior of the E_b/N_0 data from December 2014 (Figure 7) that differs so much from the rest of the data (Figures 8 to 27) may be attributed to testing that may have occurred during this very short time period. In any event, the bulk of the data lies along the favorable link curve and only 0.2 percent lies below the 3-dB dashed yellow curve (see first entry in Table 1).

It is noteworthy to point out that all the usable data since 2015-305 occurs at elevation angles above 20 deg (Figures 13 to 27). However, data prior to this date involved observations that fall below 20 deg (see Figures 7 to 12). This may have been due to a decision by the LRO project to limit all future observations above elevation angles of 20 deg.

Another noteworthy point is that given that the rainiest months at the White Sands site are July, August, and September,[2] this correlates well with the plots that show the great-

[2] https://www.nps.gov/whsa/planyourvisit/weather.htm

Table 1. LRO E_b/N_o observation statistics.

Start Year-Day	End Year-Day	Number of Data Points	Number of Points >3 dB Curve	Percent >3 dB Curve
2014-356	2014-358	37873	37808	99.83
2015-162	2015-181	323484	321848	99.49
2015-182	2015-212	456029	452480	99.22
2015-213	2015-243	477671	474381	99.31
2015-244	2015-273	444294	442073	99.50
2015-274	2015-304	456456	449285	98.43
2015-305	2015-334	423278	421441	99.57
2015-335	2015-365	405961	403829	99.47
2016-001	2016-031	405129	401928	99.21
2016-032	2016-060	385177	383440	99.55
2016-061	2016-091	414459	413296	99.72
2016-092	2016-121	410079	408439	99.60
2016-122	2016-146	353394	350796	99.26
2016-161	2016-219	707538	702600	99.30
2016-219	2016-277	672197	664049	98.79
2016-277	2016-330	718719	714964	99.48
2016-331	2017-020	679465	669964	98.60
2017-021	2017-073	675049	670357	99.30
2017-074	2017-128	712037	708782	99.54
2017-129	2017-183	696930	693105	99.45
2017-183	2017-229	548142	539454	98.42
Totals		10403361	10324319	99.24

est prevalence of connected features (likely rain fade features) lying below the adverse red curves in Figures 7 to 27. These include Figure 9 (July 2015), Figure 20 (June–August 2016), Figure 21 (August–October 2016), and Figure 27 (July–August 2017).

The removal of any non-atmospheric features in Figures 7 to 27 as well as removal of spurious pre-acquisition and post-track data in these figures will result in higher percentages of data lying above the 3-dB dashed yellow curves, which are already at the 98 to 99 percent level. Thus, we could consider the present results to be on the conservative side.

The period from January 2015 to October 2015 ranks as the second wettest January–October period on record in New Mexico.[3] It was especially wet in the southern part of New Mexico where White Sands is located. We can see several such rain events in the available LRO E_b/N_0 data from WS1 where the "stringy" signatures extend below the red adverse curves in Figures 8 to 12 for this period, and occasionally dip below the "Adverse – 3 dB" curves. As an example, we can more closely examine a couple of these features from October 2015 as seen in Figure 12, and plot these data versus time and then examine these features with available rain gauge data (see Figure 28, tracks inside purple ovals). The top

[3] https://www.abqjournal.com/675008/at-1736-inches-janoct-rainfall-average-is-second-highest-for-nm.html, Albuquerque Journal, 2015.

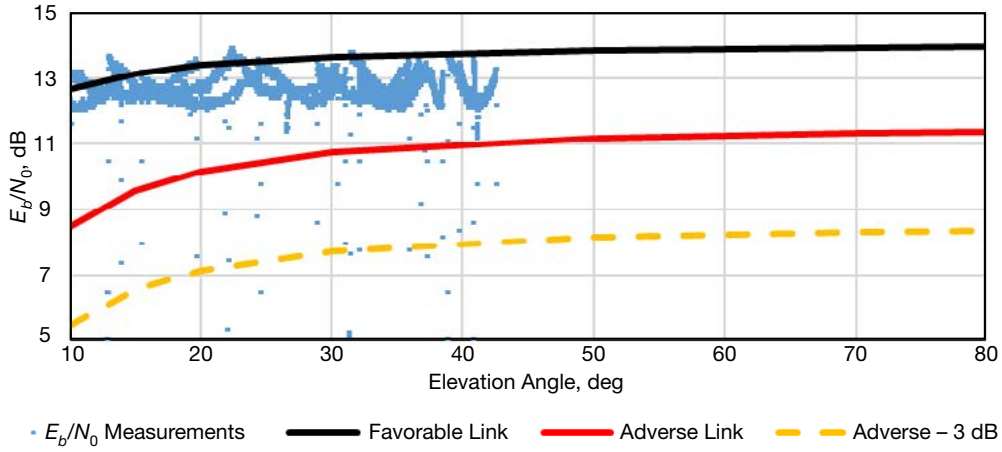

Figure 7. E_b/N_0 vs. elevation angle — December 2014 (2014-356 to 2014-358).

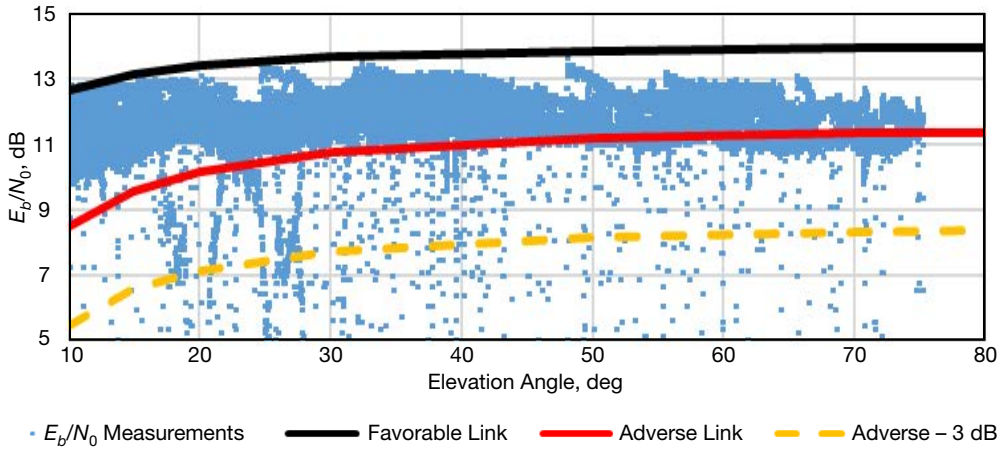

Figure 8. E_b/N_0 vs. elevation angle — June 2015 (2015-162 to 2015-181).

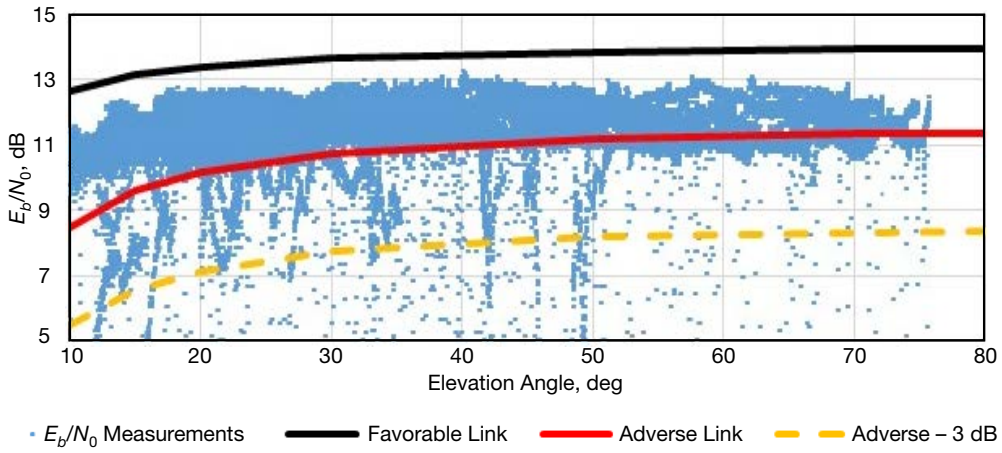

Figure 9. E_b/N_0 vs. elevation angle — July 2015 (2015-182 to 2015-212).

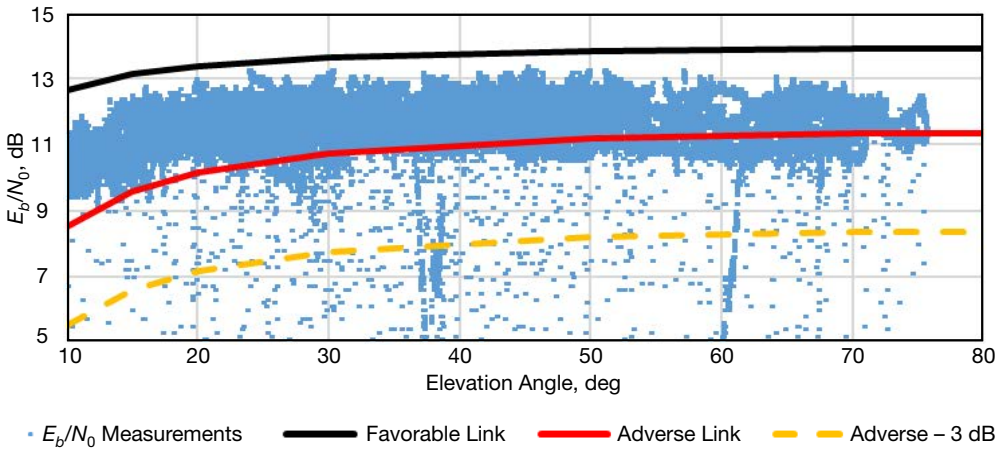

Figure 10. E_b/N_0 vs. elevation angle — August 2015 (2015-213 to 2015-243).

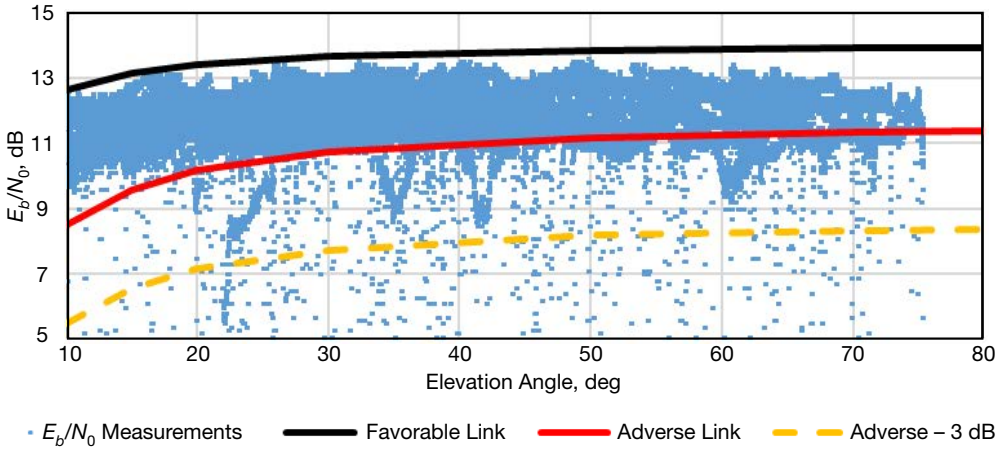

Figure 11. E_b/N_0 vs. elevation angle — September 2015 (2015-244 to 2015-273).

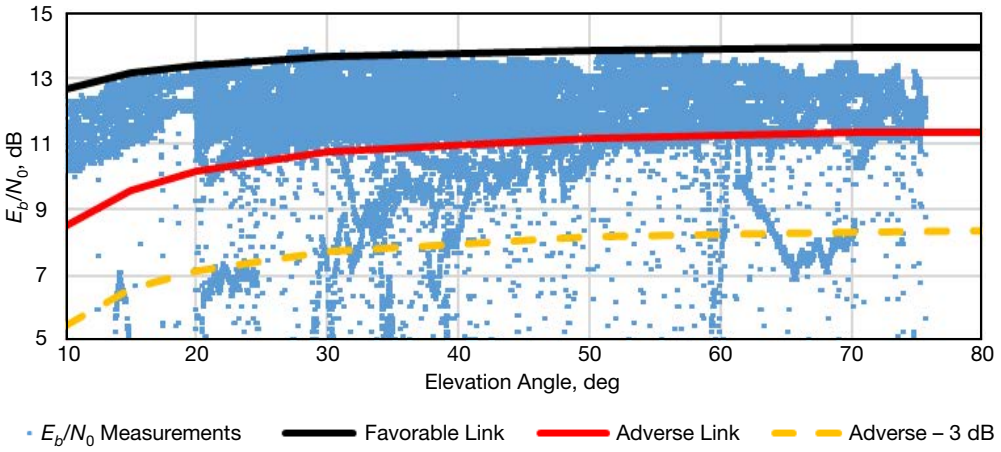

Figure 12. E_b/N_0 vs. elevation angle — October 2015 (2015-274 to 2015-304).

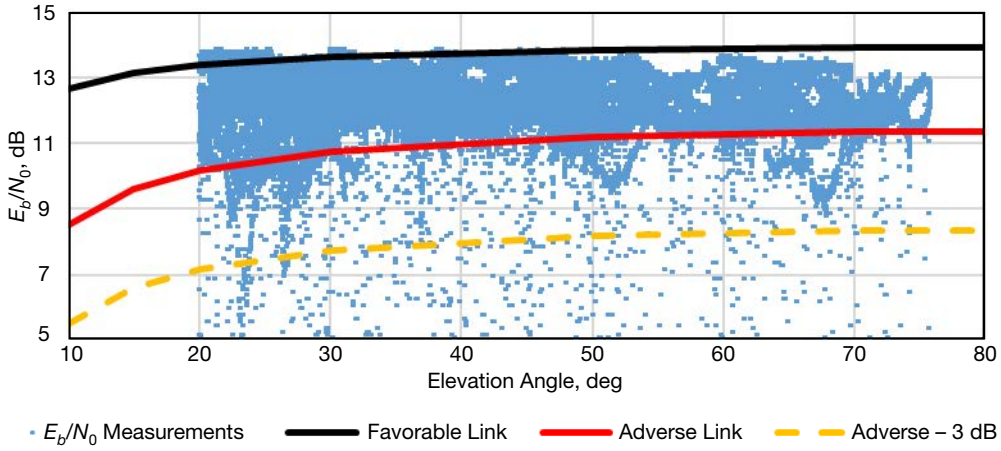

Figure 13. E_b/N_0 vs. elevation angle — November 2015 (2015-305 to 2015-334).

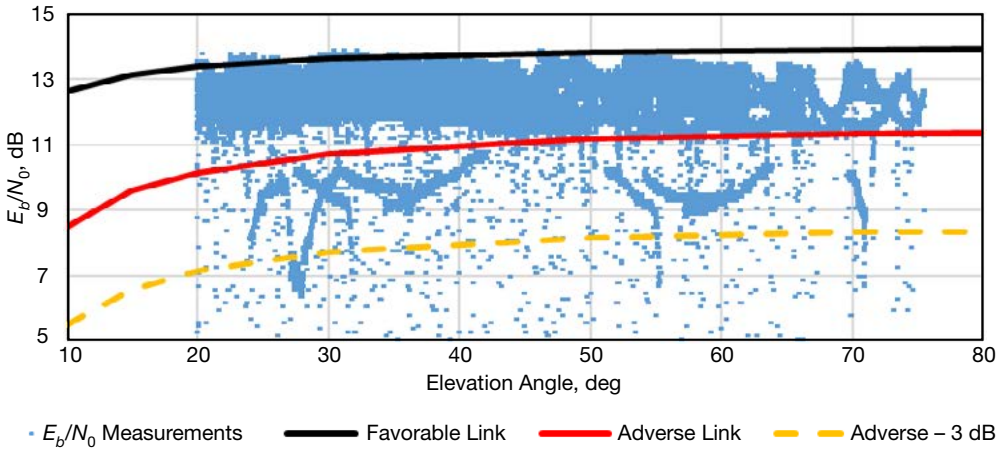

Figure 14. E_b/N_0 vs. elevation angle — December 2015 (2015-335 to 2015-365).

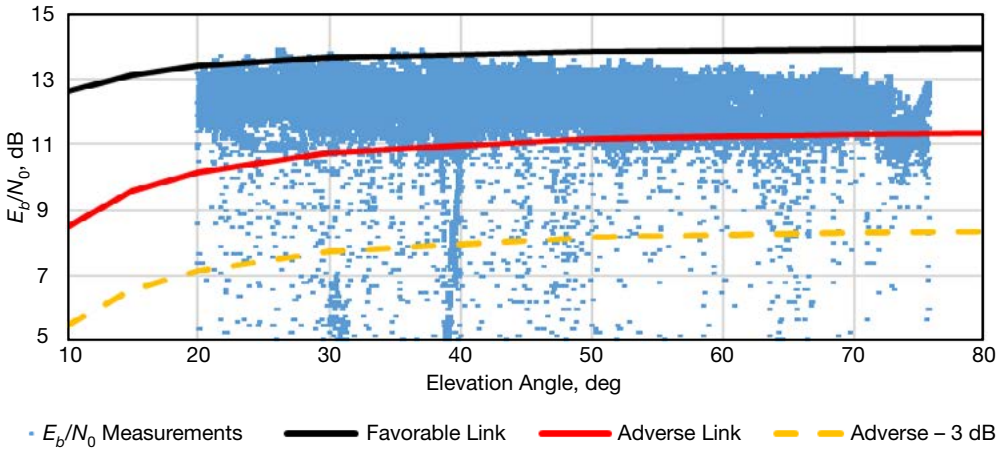

Figure 15. E_b/N_0 vs. elevation angle — January 2016 (2016-001 to 2016-031).

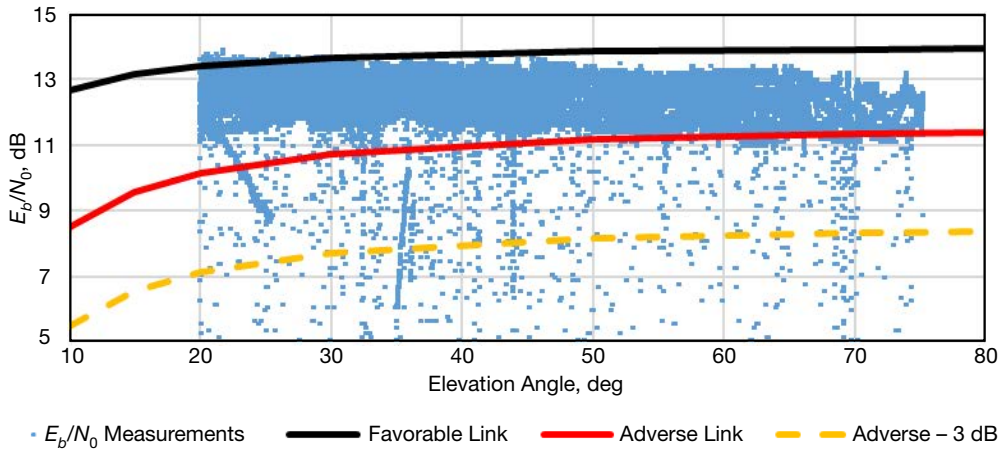

Figure 16. E_b/N_0 vs. elevation angle — February 2016 (2016-032 to 2016-060).

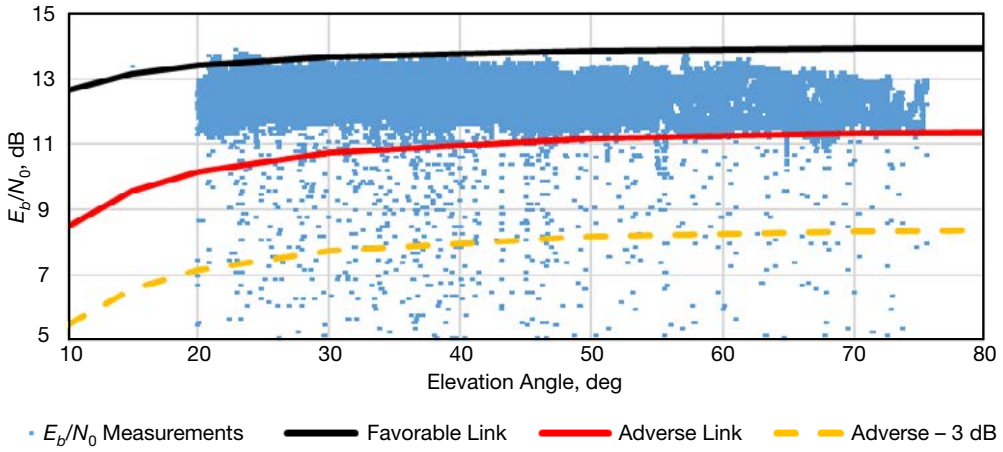

Figure 17. E_b/N_0 vs. elevation angle — March 2016 (2016-061 to 2016-091).

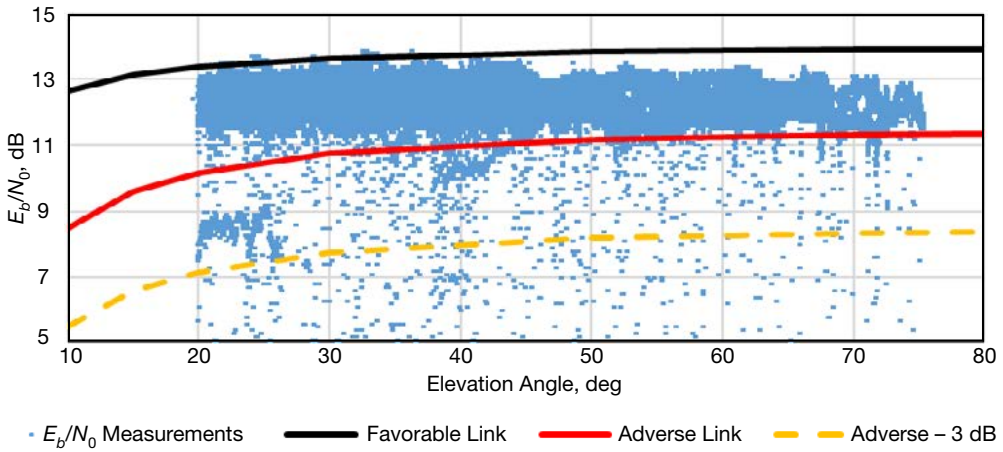

Figure 18. E_b/N_0 vs. elevation angle — April 2016 (2016-092 to 2016-121).

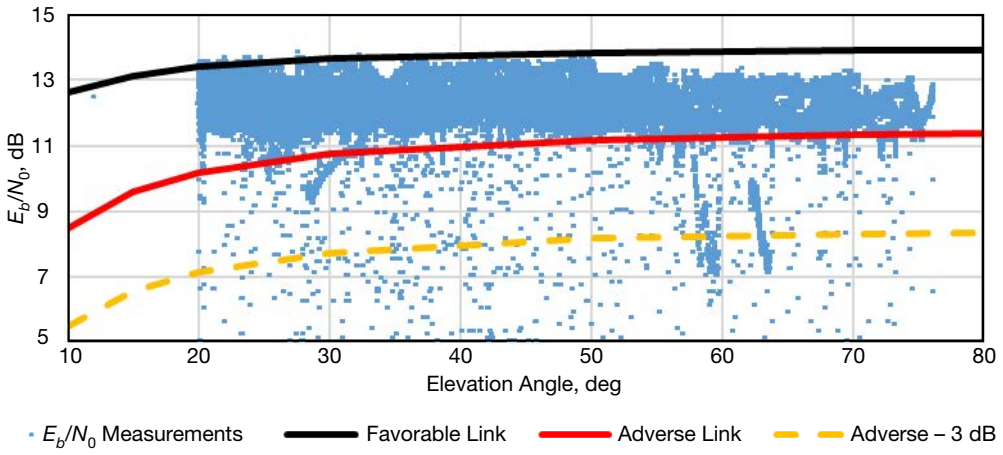

Figure 19. E_b/N_0 vs. elevation angle — May 1, 2016, to May 25, 2016 (2016-122 to 2016-146).

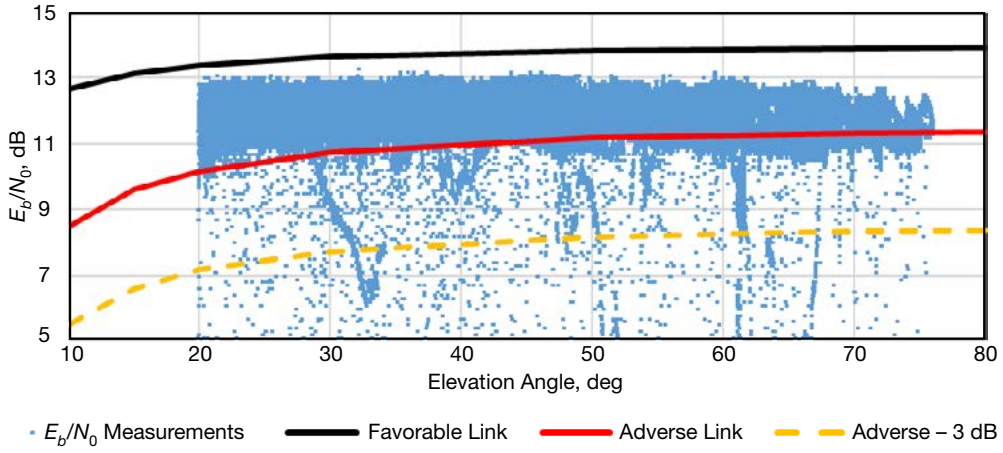

Figure 20. E_b/N_0 vs. elevation angle — June 9, 2016, to August 6, 2016 (2016-161 to 2016-218).

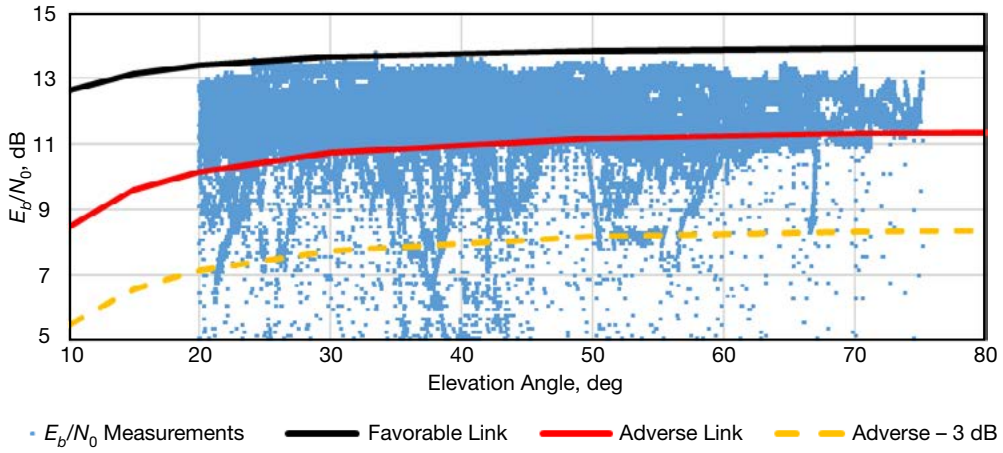

Figure 21. E_b/N_0 vs. elevation angle — August 7, 2016, to October 3, 2016 (2016-219 to 2016-276).

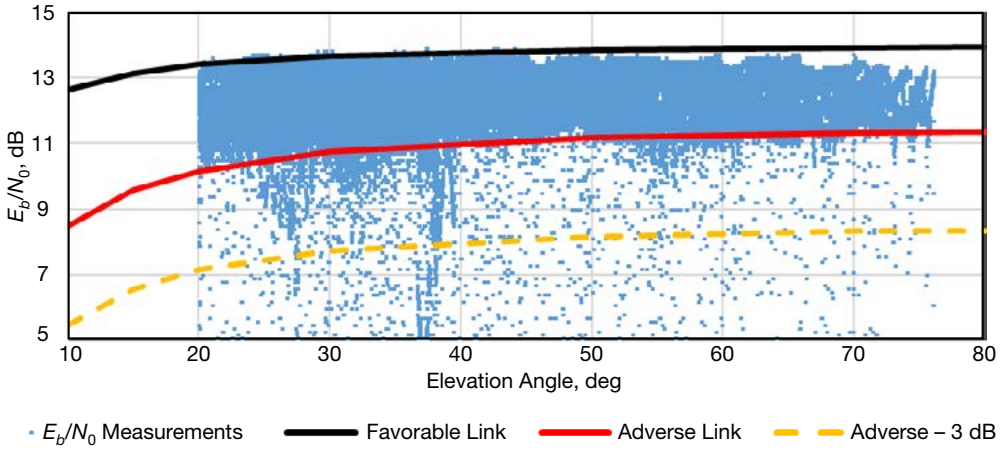

Figure 22. E_b/N_0 vs. elevation angle — October 4, 2016, to November 25, 2016 (2016-277 to 2016-330).

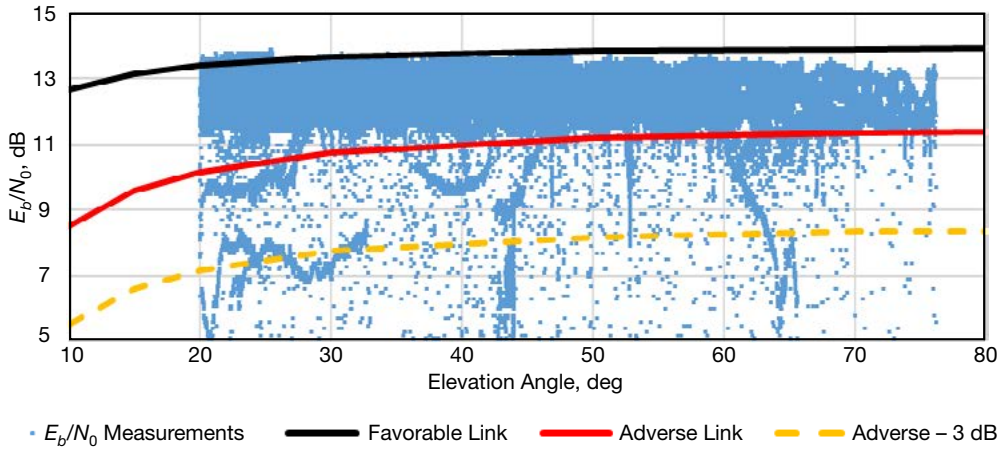

Figure 23. E_b/N_0 vs. elevation angle — November 26, 2016, to January 20, 2017 (2016-331 to 2017-020).

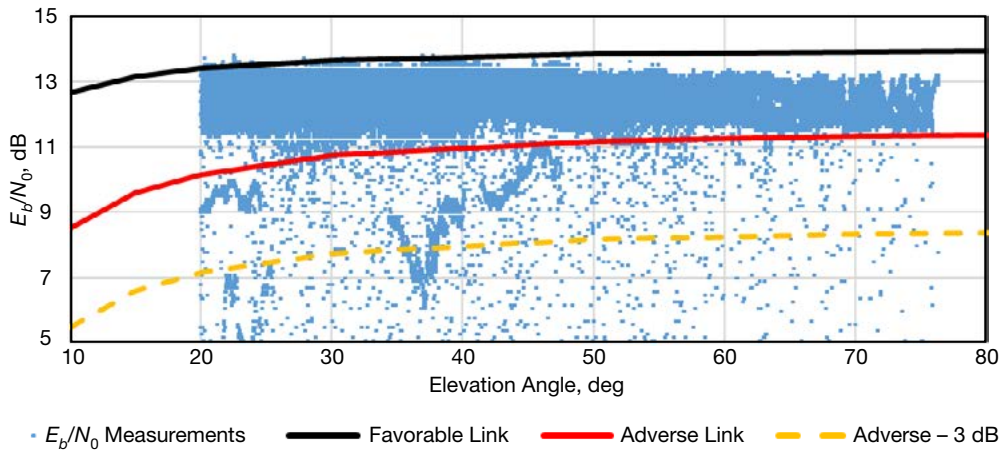

Figure 24. E_b/N_0 vs. elevation angle — January 21, 2017, to March 14, 2017 (2017-021 to 2017-073).

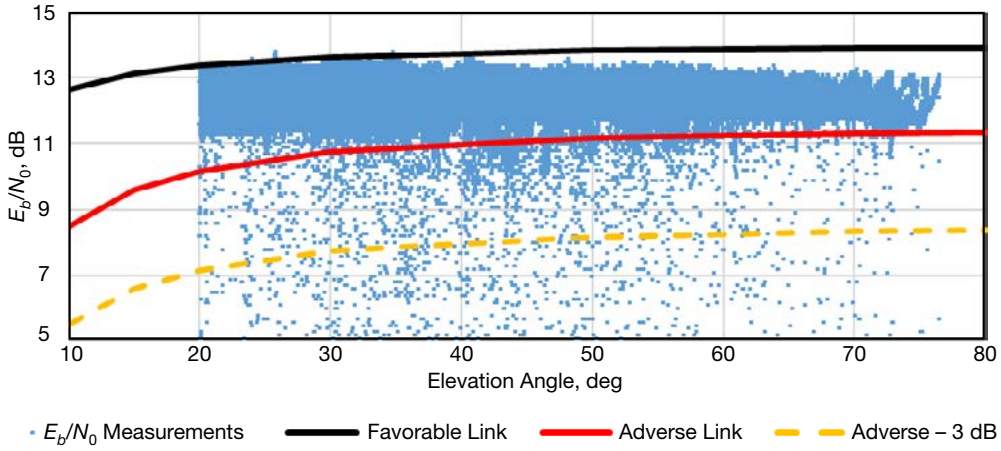

Figure 25. E_b/N_0 vs. elevation angle — March 15, 2017, to May 8, 2017 (2017-074 to 2017-128).

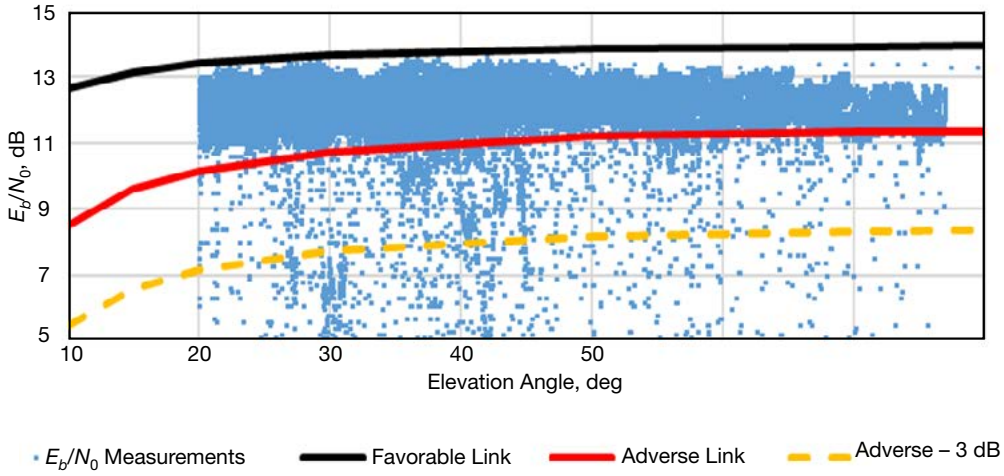

Figure 26. E_b/N_0 vs. elevation angle — May 9, 2017, to July 2, 2017 (2017-129 to 2017-183).

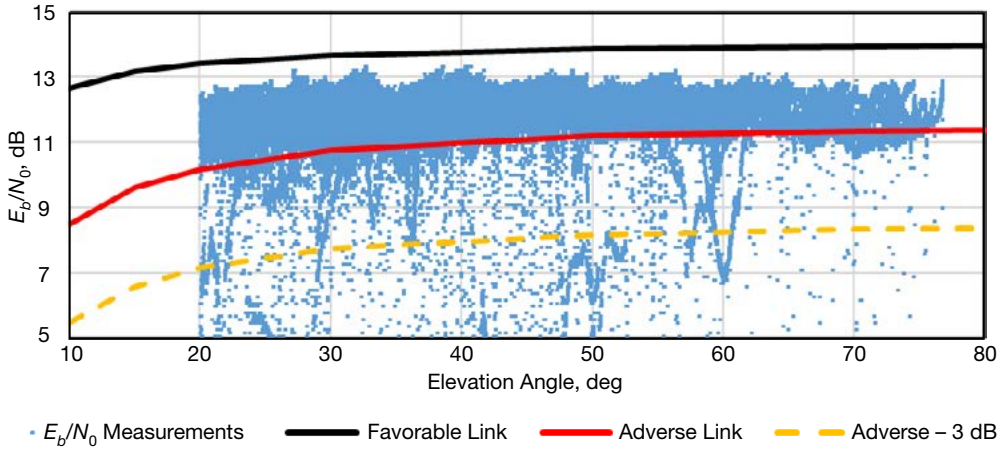

Figure 27. E_b/N_0 vs. elevation angle — July 2, 2017, to August 17, 2017 (2017-183 to 2017-229).

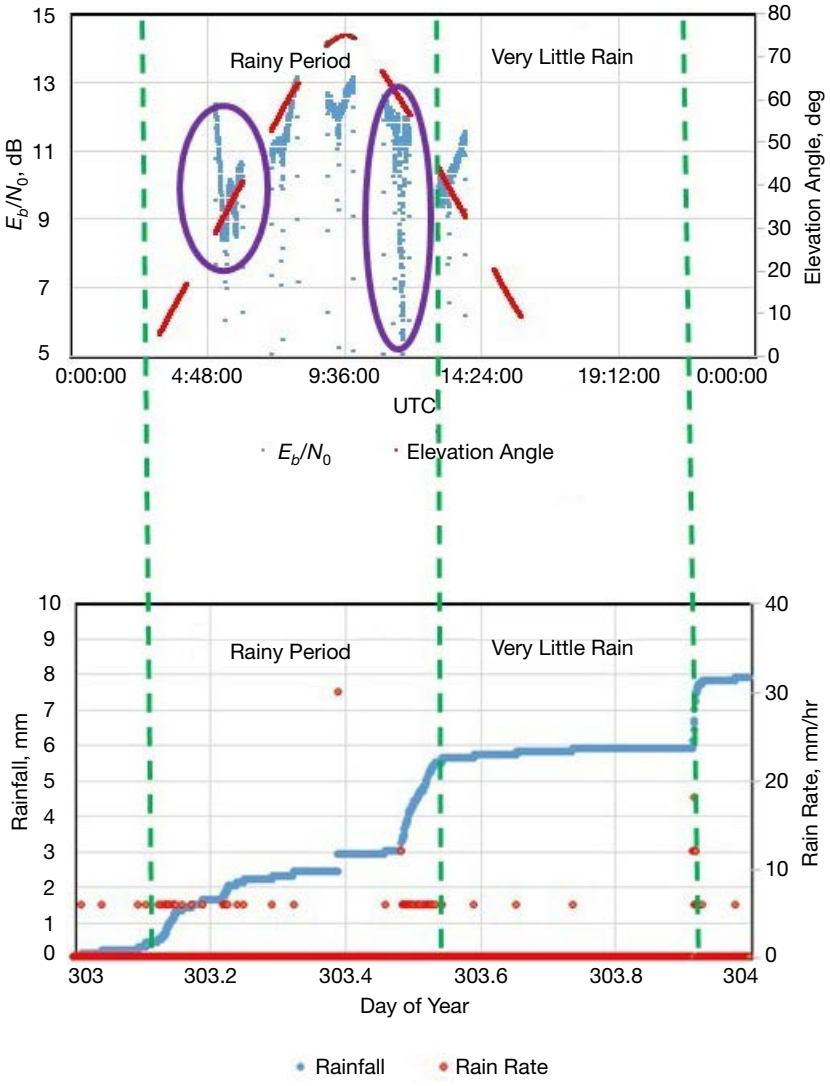

Figure 28. The top plot displays the E_b/N_0 versus time for five tracks conducted during a one-day period (October 30, 2015). The bottom plot displays the rain rate and accumulated rainfall data for the same period. Horizontal axes have different labels but cover the same period.

plot in Figure 28 displays the E_b/N_0 versus time for five tracks conducted during a one-day period, while the bottom plot displays the rain rate and accumulated rainfall data for the same period. There are clearly degraded fade features that correlate with periods of higher rain rate (red) and increasing accumulated rainfall slope (blue), primarily during the first and fourth tracking passes whose data are enclosed by the purple ovals.

Figure 29 displays the correlation of E_b/N_0 fades against rain data for another period from December 12, 2015. For this case, we examined the reduced E_b/N_0 signature lying below 10 dB extending down to near 6.5 dB between 25 deg and 30 deg elevation angle in Figure 14. The data were then plotted against time along with those of three other tracks that followed this pass (see top plot in Figure 29). The upper plot thus shows the time series for this pass (inside purple oval) along with that of the three subsequent passes (which appear

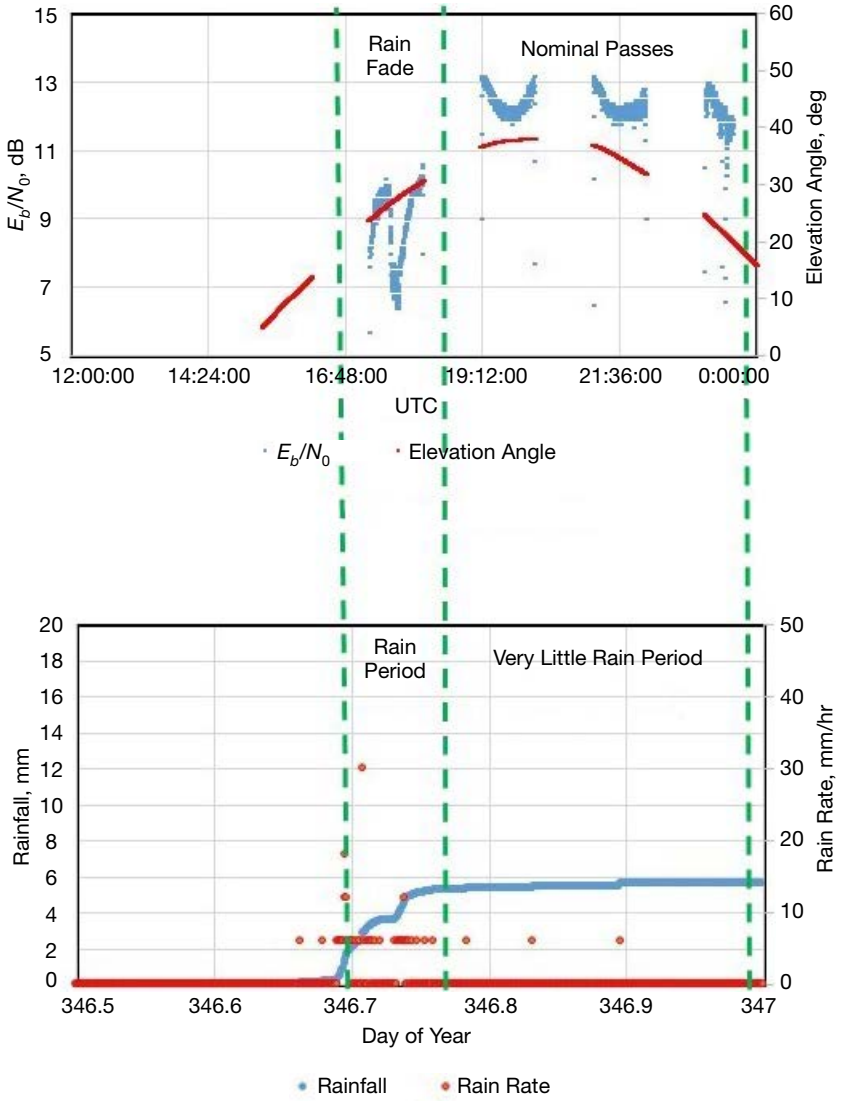

Figure 29. The top plot displays the E_b/N_0 versus time for four tracks conducted during a 12-hr period on December 12, 2015. The bottom plot displays the rain rate and accumulated rainfall data for the same period. Horizontal axes have different labels but cover the same period.

nominal). Rain data were then retrieved from a sensor located near the WS1 antenna used for reception of the signal. The bottom plot in Figure 29 displays the rain gauge data from this sensor lying below the upper plot of E_b/N_0 versus time plot. Although the horizontal time axes of both plots are labeled differently, they span the same time-period. Figure 29 clearly shows that the first pass with the rain fade event coincides with the period of persistent non-zero rain rate (red points) and increasing rainfall (blue points). The rain ceases soon after this pass. The remainder of the passes conducted during this day appear to have nominal signatures, as there are very few non-zero rain rate measurements (red points), with the total rainfall leveling off (flat signature of blue points).

A significant fraction of the scattered data points (non-connected features) appearing below the Adverse and "Adverse – 3 dB" curves in Figures 7 to 27 are attributable to wind-induced

effects on the mechanical structure of the ground antenna. High winds will tend to induce pointing variations, which in turn causes degradation in received signal strength, causing the lower E_b/N_0 measurements. Figure 30 provides examples of tracking passes for five successive orbits, which allow us to visually inspect this correlation between wind speed (red points) and degradation in received E_b/N_0 (blue points). We see that for the first two tracks where the wind speeds are relatively low, the E_b/N_0 measurements exhibit very little scatter, which mostly appears at the end or beginning of each track. For the last three tracks where the wind speeds approach, and at times, exceed 40 mph, there is appreciable scatter in the E_b/N_0 measurements where many points lie below E_b/N_0 ~11 dB, all the way down to 5 dB (the bottom scale of the plot). The LRO link documentation [3] specifies a pointing loss of "up to 2 dB," but evidently can exceed this based on the results of this analysis. Similar such behavior has been observed on deep-space Ka-band (32-GHz) signal data from the Kepler spacecraft using a 34-m-diameter antenna during high winds (see the companion article in this volume [2]).

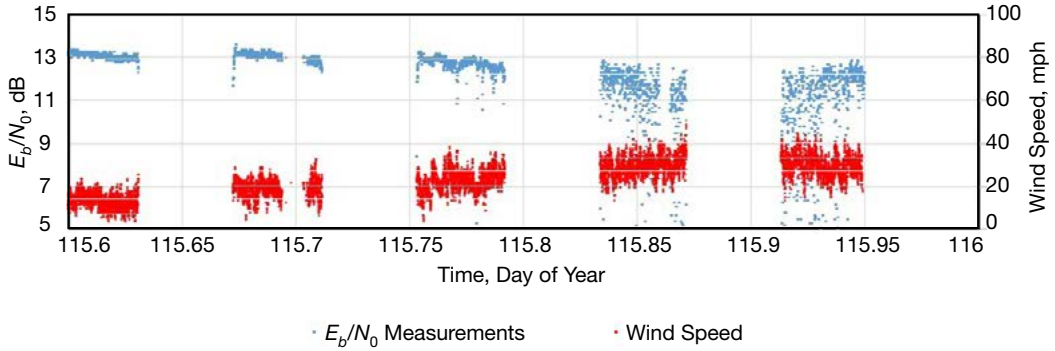

Figure 30. Received E_b/N_0 (blue points) and wind speed (red points) during the latter half of April 25, 2017 (day of year 115).

After conducting similar examinations of much of the data lying below the "Adverse – 3 dB" curves in Figures 7 to 27, we find that many of the "stringy" connected-point signatures appear correlated with periods of significant rainfall, and many of the scattered points appear correlated with periods of high winds. We therefore conclude that much of the observed degradation in E_b/N_0 data lying below the adverse curves in Figures 7 to 27 are likely atmospheric in nature (both due to moisture and winds). The statistics presented in Table 1 show that ~99 percent of the E_b/N_0 measurements lie above the "Adverse – 3 dB" curves in Figures 7 to 27. We believe that the subsequent identification and removal of any residual non-atmospheric-induced degraded data (such as slews due to antenna mispointing) will not significantly affect the statistics and indeed will increase the percentage of data lying above these curves. A more detailed and complete analysis is a subject for future study.

Data continuity is not the only customer value, as some customers also value data volume. A future study will incorporate a cumulative distribution function (CDF) analysis, which would yield a recommendation as to the margin to use for best data volume. In the meantime, this present study has a limitation as it lacks a data volume analysis. This task has been identified as a focus of future study when a more detailed analysis will be performed on the full data set where all measurements will be adjusted to a common range distance, including removal of lunar hotbody noise. Prediction of data volume return as a function

of orbit projection at lower frequency bands for LRO-type missions taking into account hotbody noise signatures was a subject of a previous study [7].

Although the favorable and adverse curves apparently do a reasonable job of bounding the main envelope defined by the E_b/N_0 observations versus elevation angle, they do not agree fully with statistical expectations. For example, we expected more observations to lie above the favorable curve in certain cases. Such an analysis is the focus of further study such as when all observations can be adjusted to a common range distance with the hotbody noise contribution removed, and further data editing performed to remove any non-atmospheric features.

IV. Conclusion

This article reports on the analysis findings of over 10 million observations of received signal strength from the LRO spacecraft collected between 2014 and 2017 at White Sands. We analyzed these data to characterize link performance over a wide range of weather conditions, season, and as a function of elevation angle. These results show that a 3-dB margin with respect to adverse link budget assumptions will ensure a ~98 to 99 percent data return under 95 percent weather conditions at 26 GHz (K-band), thus confirming expectations from link budget predictions. One finds that the 3-dB margin is applicable over elevation angles at 10 deg and above. Thus, missions that have sufficient power for their desired data rates may opt to use 10 deg as their minimum elevation angle. Limitations of this study include climate variability and the fact that the observations require removal of hotbody noise in order to perform an adequate CDF analysis, which is planned for a future comprehensive study. Flight projects may use other link margins depending upon available information, uncertainties of non-atmospheric link parameters, and mission phase.

Upcoming missions such as the Joint Polar Satellite System (JPSS); NASA–ISRO Synthetic Aperture Radar (NISAR); and Plankton, Aerosol, Cloud, ocean Ecosystem (PACE) will be downlinking K-band signals to high-latitude ground terminals whose climates are more amenable to K-band signals. The antenna structures will be enclosed inside radomes to protect against the impact of wind. The ground supports will be baselined to a minimum elevation angle of 10 deg. The link design will include atmospherics based on the current ITU models for those specific locations. Signal strength measurements will be acquired in a similar manner as done for LRO, so that a similar analysis can be performed in the future.[4]

Acknowledgments

We thank Barry Geldzahler, Faramaz Davarian, Kar-Ming Cheung, and Jon Hamkins for their support of this work. We acknowledge the assistance of Ralph Casasanta of NASA Goddard Space Flight Center (GSFC) LRO Ground Station and Operation and Engineering Support for arranging the delivery of the data sets and for promptly addressing questions as they arose. We acknowledge Harvey Elliott (Space Communications Network Services Soft-

[4] Frank Stocklin, personal communication, NASA Goddard Space Flight Center, Greenbelt, Maryland, October 20, 2017.

ware Engineer at NASA Wallops Flight Facility) for his assistance in recovering and delivering archived data sets and promptly addressing questions as they arose. We also thank Frank Stocklin of GSFC and Asoka Dissanayake of Harris Corp. for very valuable comments and recommendations. We thank James Nessel of NASA Glenn Research Center for providing some of the weather data used in the correlation analysis. Finally, we thank Julian Breidenthal for his meticulous review of the article.

References

[1] D. D. Morabito, D. Kahan, K. Oudrhiri, and C.-A. Lee, "Cassini Downlink Ka-Band Carrier Signal Analysis," *The Interplanetary Network Progress Report*, vol. 42-208, Jet Propulsion Laboratory, Pasadena, California, pp. 1–22, February 15, 2017. http://ipnpr.jpl.nasa.gov/progress_report/42-208/208B.pdf

[2] D. D. Morabito, "Deep Space Ka-Band Flight Experience," *The Interplanetary Network Progress Report*, vol. 42-211, Jet Propulsion Laboratory, Pasadena, California, pp. 1–16, November 15, 2017. http://ipnpr.jpl.nasa.gov/progress_report/42-211/211B.pdf

[3] *Radio Frequency Interface Control Document (RFICD) Between Lunar Reconnaissance Orbiter (LRO) and the Near-Earth Network (NEN), Deep Space Network (DSN), and Space Network (SN)*, Revision 1, 450-RFICD-LRO/NEN/DSN/SN, NASA Goddard Space Flight Center, Greenbelt, Maryland, Publication Date: February 2009, Expiration Date: February 2014.

[4] D. D. Morabito, "A Comparison of Estimates of Atmospheric Effects on Signal Propagation Using ITU Models: Initial Study Results," *The Interplanetary Network Progress Report*, vol. 42-199, Jet Propulsion Laboratory, Pasadena, California, pp. 1–24, November 15, 2014. http://ipnpr.jpl.nasa.gov/progress_report/42-199/199D.pdf

[5] C. Ho, A. Kantak, S. Slobin, and D. Morabito, "Link Analysis of a Telecommunication System on Earth, in Geostationary Orbit, and at the Moon: Atmospheric Attenuation and Noise Temperature Effects," *The Interplanetary Network Progress Report*, vol. 42-168, Jet Propulsion Laboratory, Pasadena, California, pp. 1–22, February 15, 2007. http://ipnpr.jpl.nasa.gov/progress_report/42-168/168E.pdf

[6] D. D Morabito, "Lunar Noise-Temperature Increase Measurements at S-Band, X-Band, and Ka-Band Using a 34-Meter-Diameter Beam-Waveguide Antenna," *The Interplanetary Network Progress Report*, vol. 42-166, Jet Propulsion Laboratory, Pasadena, California, pp. 1–18, August 15, 2006. http://ipnpr.jpl.nasa.gov/progress_report/42-166/166C.pdf

[7] D. D. Morabito, "Dynamic Telemetry Link Advantage When Tracking a Lunar Orbiter with a 34-m Antenna at 2.3 GHz and 8.4 GHz," *The Interplanetary Network Progress Report*, vol. 42-200, Jet Propulsion Laboratory, Pasadena, California, pp. 1–17, February 15, 2015. http://ipnpr.jpl.nasa.gov/progress_report/42-200/200C.pdf